Real-Time Observation of Iodide Ion Migration in Methylammonium Lead Halide Perovskites

Cheng Li[1)], Antonio Guerrero[2)], Yu Zhong[1)], Anna Gräser[1)], Carlos Andres Melo Luna[3,4)], Juan Bisquert[2)], Richard Hildner[3)], Sven Huettner[1, a)]

Abstract

Organic-inorganic metal-halide perovskites (*e.g.* $CH_3NH_3PbI_{3-x}Cl_x$) emerged as a promising opto-electronic material. However, the Shockley–Queisser Limit for the power conversion efficiency (PCE) of perovskite-based photovoltaic devices has still not been reached, which was attributed to non-radiative recombination pathways, as suggested by photoluminescence (PL) inactive (or dark) areas on perovskite films. Although these observations have been related to the presence of ions/defects, the underlying fundamental physics and detailed microscopic processes, concerning trap/defect status, ion migration, *etc*., still remain poorly understood. Here we utilize correlated wide-field PL microscopy and impedance spectroscopy (IS) on perovskite films to *in-situ* investigate both the spatial and temporal evolution of these PL inactive areas under external electrical fields. We attribute the formation of PL inactive domains to the migration and accumulation of iodine ions under external fields. Hence we are able to characterize the kinetic processes and determine the drift velocities of these ions. In addition, we show that I_2 vapor directly affects the PL quenching of a perovskite film, which provides evidence that the migration/segregation of iodide ions plays an important role in the PL quenching and consequently limits the PCE of organometal halide based perovskite photovoltaic devices.

1) Organic and Hybrid Electronics, Macromolecular Chemistry I, University of Bayreuth, Universitätstr. 30, 95447 Bayreuth, Germany
2) Institute of Advanced Materials (INAM), Universitat Jaume I, 12006 Castelló, Spain
3) Experimental Physics IV and Bayreuth Institute of Macromolecular Research, University of Bayreuth, Universitätstr. 30, 95447 Bayreuth, Germany
4) Centre for Bioinformatics and Photonics – CIBioFi, Calle 13 No. 100-00, Edificio 320 No. 1069 and Departamento de Fisica, Universidad del Valle, 760032 Cali, Colombia
a) Authors to whom correspondence should be addressed. Electronic addresses: sven.huetttner@uni-bayreuth.de

1. Introduction

Inorganic-organic halide organometal perovskite solar cells (*e.g.* $CH_3NH_3PbI_{3-x}Cl_x$ and $CH_3NH_3PbI_3$) have achieved remarkable power conversion efficiencies (PCE) in the last few years, jumping from 3.8%[1] to more than 20%.[2] Yet, quite a lot of fundamental physics in this material is still under debate.[3, 4] Among them, more and more concern is concentrated on the further improvement of PCE approaching the Shockley–Queisser Limit.[5]

It is well known that the PCE of solar cells is correlated with its photoluminescence (PL) property, which is an indication of the charge carrier recombination pathway.[6] Briefly, the charge carrier recombination is considered as a combined process of (1) trap/defects-assisted (first order) (2) electron-hole bimolecular (second order) and (3) Auger recombination (third order).[7, 8] To achieve the ideal maximum PCE, or the Shockley–Queisser Limit,[9] the device has to perform as a "good radiator",[10] that is, to maximize the radiative bimolecular recombination based on the detailed balance model. In reality, perovskites have demonstrated outstanding performance on the application of light emitting diodes[11] and lasers.[4, 12] Nevertheless, the appearance of dark areas, or PL inactive domains in perovskite films, have been reported.[13-18] These dark areas in PL images indicate the existence of non-radiative recombination pathways, which are detrimental to the energy conversion and can be passivated by chemical treatment.[8, 13, 19] Recently more and more evidences demonstrate that this non-radiative recombination is associated with the migration/segregation of ions in the film.[17, 20] Therefore, the study of ionic dynamic becomes an emergent issue.

Ultrafast spectroscopy has gained success on characterization of the charge carrier generation/recombination process (~ns timescale or even faster) in perovskites.[6, 21] However, the contribution of ions/defects with timescales of ~10 sec is still not fully elucidated.[18, 22, 23] In this work, correlated wide-field PL imaging microscopy[17, 24] and impedance spectroscopy (IS)[25, 26] serve as a powerful tool to investigate the ionic/electronic dynamic process in perovskite films. Furthermore, we demonstrate a method which allows to directly visualize the migration of ions within a perovskite film.

2. Results and Discussion

2.1 Wide-field Photoluminescence Microscopy

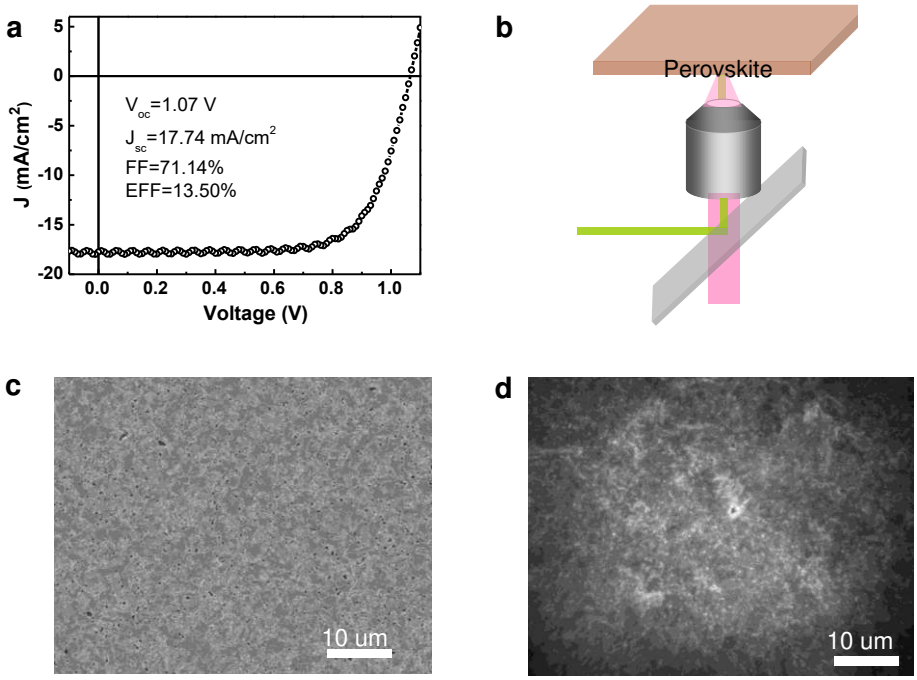

Figure 1. (a) Current density-voltage (*J-V*) curve of a perovskite solar cell under AM 1.5G illumination, with the structure depicted in Fig.S1. (b) Schematic diagram of a confocal PL imaging microscopy. (c) SEM image of a perovskite film on a glass substrate. (d) PL image of the perovskite film (not the same area). The excitation source is a 532 nm laser with an intensity of ~40 mW/cm^2, the exposure time is 50 ms.

We fabricated perovskite films for PL imaging by spin coating the mixed halide precursor solution (CH_3NH_3I:$PbCl_2$=3:1) on cleaned glass substrates followed by annealing at 100 ºC for 1 hour in a nitrogen glovebox. These films (as shown in

Figure S1)exhibit PCEs of ~13.5% (Fig 1(a)), when employed in standard solar cell device architechtures (as shown in Figure S1). Fig 1(b) depicts the schematic of a wide-field PL imaging microscope. A detailed description has been reported previously.[27] Briefly, we use a home-built optical microscope, which can be operated using wide-field illumination and a charge-coupled device (CCD) camera as a detector to obtain PL images of large areas (diameter ~60 μm) of a sample. We are able to record typically sequences of up to 2000 PL images with exposure times as short as 50 ms per image. This enables us to track the temporal/spatial evolution of the PL intensity from a perovskite film under continuous laser illumination. Figure 1 (c) illustrates the scanning electron microscopy (SEM) image of a perovskite film on glass, while Figure 1 (d) is the PL image of the same film on a similar scale (yet not of the same region). The SEM image in Fig 1(c) shows the perovskite film possesses densely packed grains ranging from 100 nm to 800 nm in size (Figure S2), which is consistent with the PL image (Fig 1(d)). We note that on the surface of the device, the spatial distribution of the PL intensity is not uniform. This may be ascribed to the inhomogeneous distribution of composition and defects. Note that it has been reported that the presence of oxygen and moisture may result in a significant increase of the PL.[15, 28] Here, to rule out the influence of ambient atmosphere, we deposited a polymethyl methacrylate (PMMA) layer with ~200 nm thickness on top of the perovskite film as a protection layer. In addition, the device was in direct contact with the microscope immersion oil during the whole PL characterization.

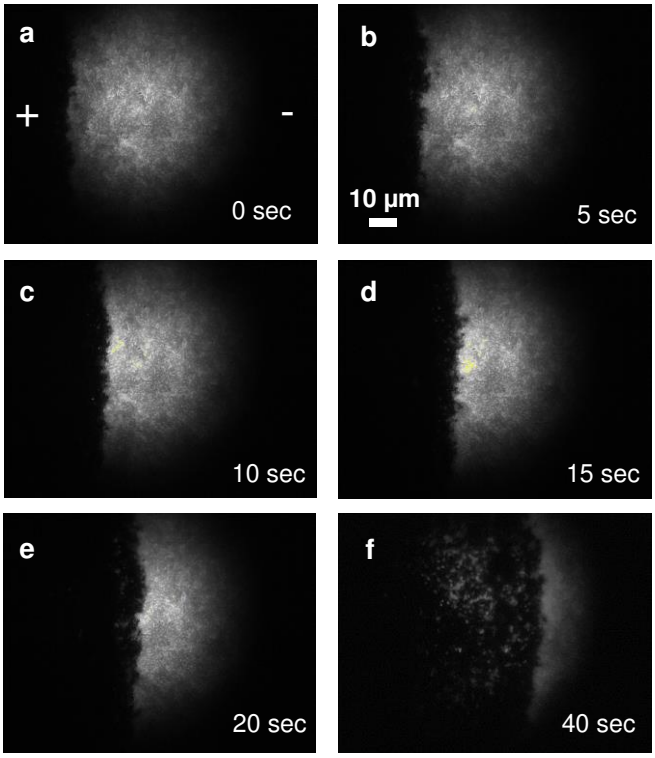

Figure 2. Time dependent PL images of a perovskite film under an external electrical field (~10^5 V/m). The '+' and '-' signs indicate the polarity of the electrodes. The excitation intensity is ~40 mW/cm^2 and the exposure time per image is 50 ms. The scale bar represents 10 µm.

It has been proposed that the migration/segregation of ions plays an important role on the decay of PL intensity.[14, 16, 18, 20, 29] These ions can be driven by an external electrical field. Therefore, we recorded time dependent PL images on films with laterally interdigitated electrodes with channel lengths of ~ 200 µm (see Fig. 2 and inset in Fig. 3). Applying a constant electric field of ~10^5 V/m, we observe that initially the PL intensity in the bright areas exhibits a uniform decrease as the device is connected with the external electrical circuit (Fig S4). This is attributed to the charge extraction by the external electrical field, which decreases the population of photogenerated charge carriers. Interestingly, under the constant electrical field, a front forms that separates bright and dark domains and that moves from the positive electrode towards the negative one, as shown sequentially in Figure 2.

Note, that in the immediate vicinity on the bright side of the migrating front (Fig 2(c) and (d) for instance), the PL intensity is abnormally high. This implies that at this boundary an electrochemical reaction occurs (see below). Taking into account the direction of the front, from positive towards negative electrode, we assign this movement of PL dark area is attributed to the migration/accumulation of negative ions, that is, iodide ions in perovskite.[14, 17] This observation is consistent with previous studies on the ionic migration, in which iodide ions serve as a main contribution for the hysteresis behavior[25, 30-32] and field driven degradation.[33, 34] As shown in Figure 2, it takes ~50 sec to turn the whole PL image (diameter is around 60 μm) to dark area, under the electrical field of 10^5 V/m. Therefore, the analysis of the kinetics of the migrating front enables to directly estimate the velocity of ionic migration.

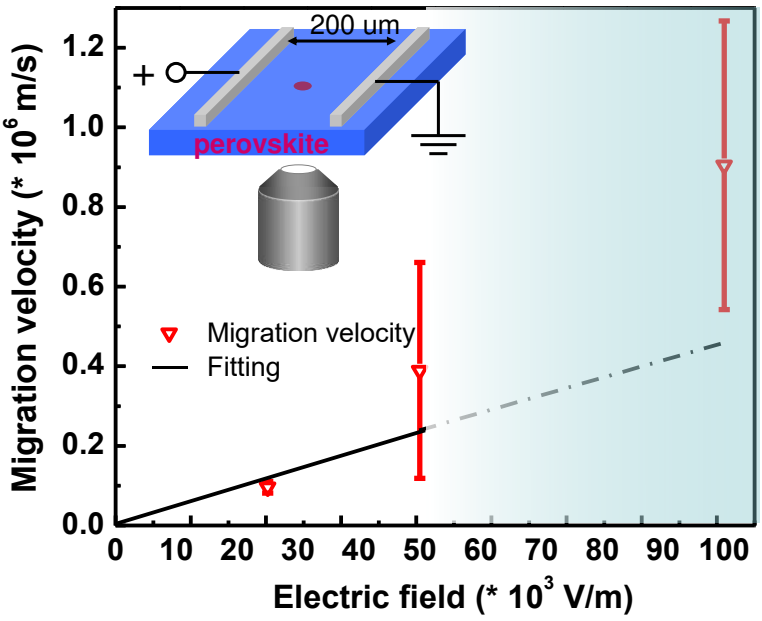

Figure 3. Field dependence of the ionic migration velocity. Inset: the schematic diagram of the setup. The black line is the fitting line based on first two points (lower voltages) considering the weight of error. Dased line is the extension of the fitting line, because at high voltage, the perovskite film exhibits decomposition (See Fig S5). The gradient colour indicates the more chemical decomposition under higher voltage.

To investigate this ionic motion, we characterize the velocity of the migrating front as a function of external electrical field. By varying the strength of the field, we obtain that the migration velocity is proportional to the field within the error, as shown in Fig

3. Ignoring the ion diffusion, this movement of the front can be described by a simple ionic mobility theory:[35]

$$v = \mu E \quad (1)$$

Here, v is the drift velocity of ion movement, μ is the mobility of ions, and E is the electrical field across the whole channel. By fitting the field dependent ionic migration (two lower voltages), the mobility of iodide ions is obtained $(5\pm2)\times10^{-12}$ m^2/Vs. This value is close to the ionic migration mobility obtained in $CH_3NH_3PbI_3$[33, 36], the discrepancy between th two values (one order of magnitude difference) may be due to the different defect density, film fabrication process (using $PbCl_2$ instead of PbI_2 as the precursor) or nature of grain boundaries. Based on the Einstein relation:[35]

$$D = \mu k_B T \quad (2)$$

where D is the diffusion constant, k_B is Boltzmann's constant and T is the absolute temperature,we obtain the diffusion constant D of $(1.0\pm0.4)\times10^{-13}$ m^2/s, which also agrees with the value $\sim10^{-12}$ m^2/s, obtained by Yang et al.[37] Here, note that the last point (1×10^5 V/m) deviates from the fitting line. This is attributed to the degradation of the perovskite film under the high electrical fields, consistent with the grazing incidence wide angle x-ray scattering (GIWAXS) results performed under different electrical fields (Fig. S5).

To further understand ionic motion within the film we reversed the bias and monitored the time evolution of the dark area. We observe that, under the reversed electrical field, the dark areas recover to the bright areas again (shown in Figure S6), although the speed of the recovering is much slower. This asymmetry may be associated with electric field induced chemical reactions,[38] and will be further addressed below. It is also observed that after 12 hours disconnected with the external

electrical field, the dark area returns to bright (not shown here). This reversible phenomenon is consistent with the iodide ion diffusion process characterized in previous papers.[17, 30]

2.2. Impedance Spectroscopy

Impedance spectroscopy (IS) has demonstrated as a powerful tool to explore the microscopic processes in perovskite solar cells, especially the migration of ionic charges.[26, 38, 39] In this work, we carried out IS measurements with the aim to electrically monitor how ions are piling up at one electrode and to correlate with the PL measurements by performing both measurements quasi-simultaneously. In a typical IS measurement a dc bias is applied to polarize the sample and a small ac perturbation is superimposed. As we have seen, ionic concentration shifts as a function of time showing a constant mobility. Therefore, the combination of the two methods allows us to implement this additional parameter in the interpretation of the IS results. The differential current output is measured which offers information on the capacitive and resistive processes taking place in an operating device. For perovskite devices it has previously been demonstrated that the response in the low frequency region is related to electrode polarization of ions by generation of a Helmholtz layer and charge compensation by the external electrode.[39]

As shown in Fig 4(a), initially a dc bias of 1V was applied in the dark to induce ion migration towards the electrodes by using a potentiostat equipped with a frequency analyzer, which is able to acquire impedance spectroscopy coupled with the PL measurements. The PL image was recorded at every end of each IS cycle (PL images shown in Figure S7). It is important to note that under this very mild field of only 1V

applied between the contacts no noticeable advance front is observed in Figure S7 in supporting information, though as established above (Fig. 3) we can assume a constant mobility. Hence, a lower voltage gives us sufficient time to carry out the respective IS cycles. Furthermore, IS measurements are very sensitive to changes at the interface level between perovskite layer and contacts. Indeed, Figure 4(a) shows the capacitance-frequency plot as a function of time. After the first IS measurement scan (7 minutes) the capacitance at low frequencies (0.1 Hz) is initially in the range of ~70 μFcm^{-2} which is a typical capacitance value produced from piling up ions at one interface due to electrode polarization.[39] Interestingly, as the polarization time increases, this low frequency capacitance decreases with lowest value observed (20 nFcm^{-2}) after 45 minutes of applied bias which could be the result of an electrochemical reaction leading to the generation of neutral species (*i.e.* PbI_2).[33]

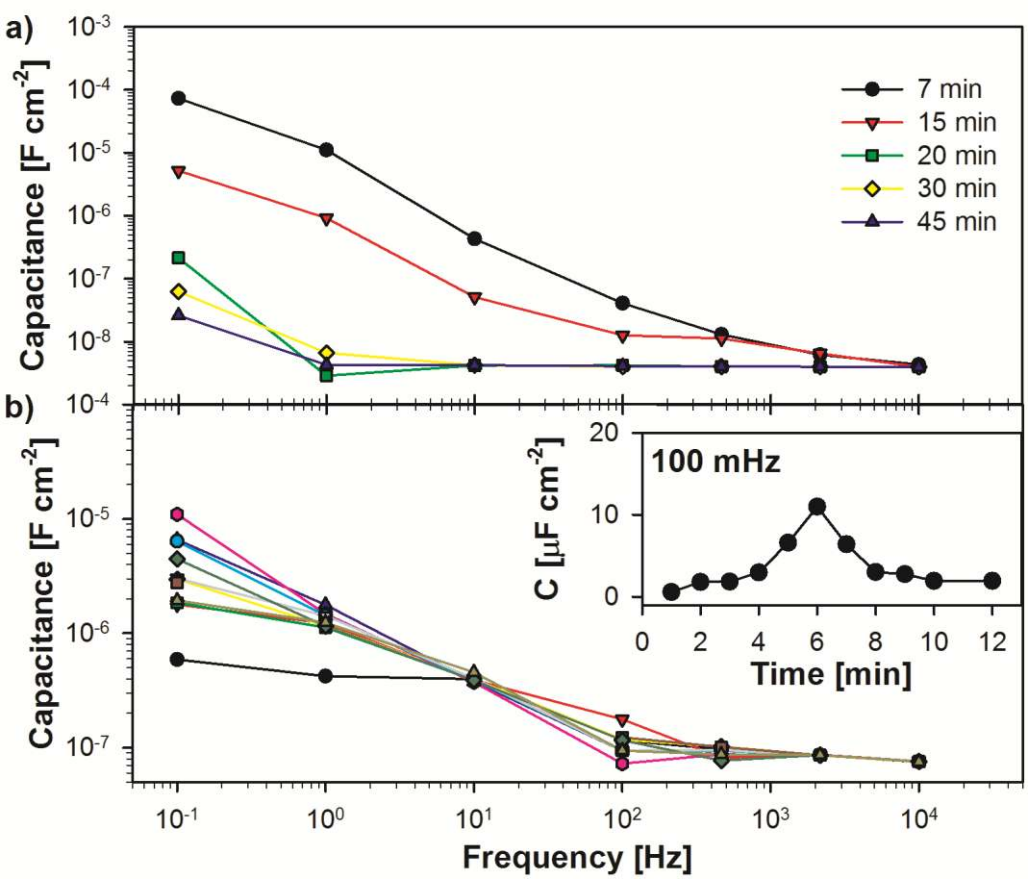

Figure 4. Capacitance-Frequency plot of measurements were carried out simultaneously during PL measurement by applying a dc bias of a) 1V and b) 2V. The inset shows the evolution of the capacitance at 100 mHz with time.

Subsequently, IS measurements were carried out with a polarization of 2 V (Figure 4(b)) with a shorter delay time (1 min). These conditions allow monitoring how the ions accumulate at one interface as a function of the time and the electrochemical reaction leading to neutral species at the electrode. Initially, the capacitance in the low frequency region is low as no ions are present in the interface (~0.7 μFcm^{-2}) and this increases with the time to reach a maximum capacitance value (10 μFcm^{-2}) observed at 6 minutes indicating that after this time most of the electrode surface is covered by charged ions that have migrated from the bulk of the perovskite layer. Note that capacitances are not as high as in the previous experiment as some of the interfacial area has already reacted in the previous experiment leading to inactive areas. After this time the capacitance begins to decrease as shown in the inset of Figure 4(b) similar to the effect observed for polarization at 1V. Capacitances of ~2 μFcm^{-2} are observed after 12 minutes of polarization indicating that the charged species covering the electrode have mostly reacted to generate neutral species.

A different set of measurements, with the same device structure, were carried out where the capacitance was measured as a function of the applied bias (Figure 5(a)) in the dark. In this set of experiments, the frequency range was increased to cover still lower frequencies (up to 5 mHz), as expected noise increases in this region as a consequence of the slow response of mobile ions to the small ac perturbation. The electrode polarization capacitance increases with the applied bias exponentially.

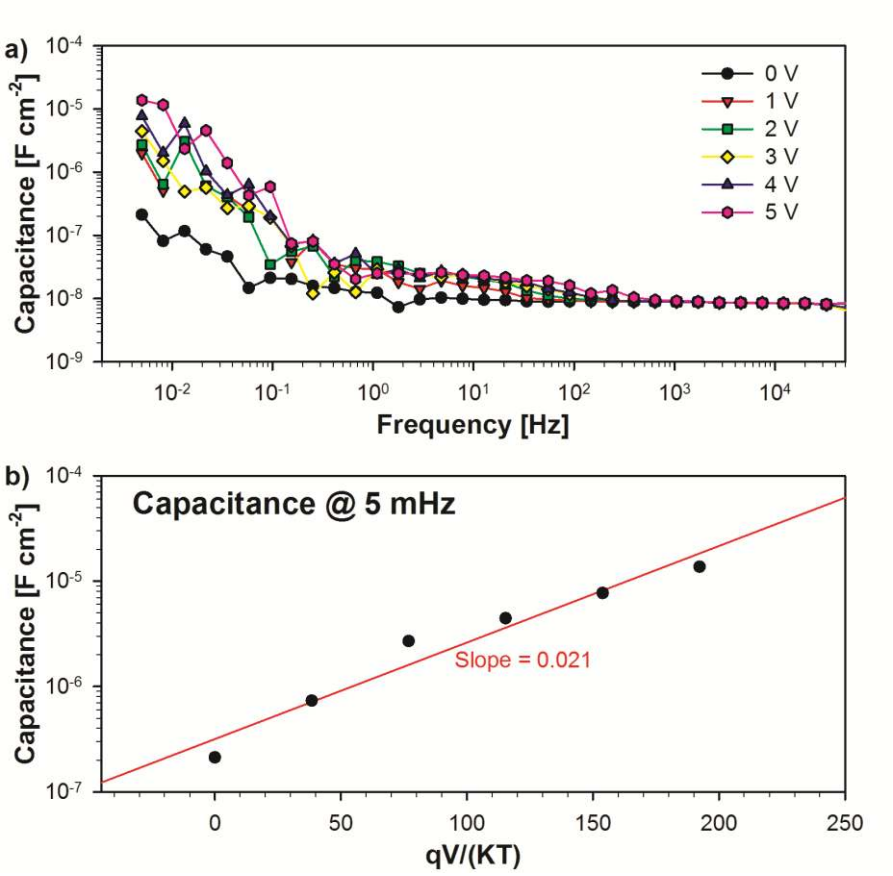

Figure 5. a) Capacitance-Frequency plot of measurements carried out in the dark as a function of the applied bias. b) Exponential relationship of capacitance as a function of external voltage measured at 5 mHz.

The observation of a variation of the capacitance with voltage, shown in Fig 5(b), is a clear indication of charge accumulation at the interface. A number of previous studies have clearly shown that the large low frequency capacitance of perovskite solar cells in the dark can originate from the mobile ion accumulation.[39, 40] In principle if the ions move freely in the solid medium the structure of the interface consists on a double layer and a diffuse layer that is controlled by the applied voltage. For a symmetric electrolyte the Gouy-Chapman model gives the capacitance[41]

$$C = \frac{\varepsilon\varepsilon_0}{L_D}\sinh\left(\frac{qV}{2k_BT}\right) \qquad (3)$$

Where V is the potential drop between the metallic contact and the absorber bulk, ε_0 is the permittivity of vacuum, ε is the dielectric constant of perovskite, and k_BT is the thermal energy, q is the charge. The ion Debye length L_D is therefore given by

$$L_D = \sqrt{\frac{\varepsilon\varepsilon_0 k_B T}{q^2 N}} \quad (4)$$

Here N accounts for the equilibrium density of ionic charges in the bulk material. Eq. (3) indicates that the extension of disequilibrium of ionic distribution at the interface is of size L_D. The capacitance at zero bias is

$$C_1 = \frac{\varepsilon\varepsilon_0}{L_D} \quad (5)$$

The thermalized distribution of ions in Eq. (3) can be approximated by the formula

$$C = C_0 e^{\frac{\alpha q V}{k_B T}} \quad (6)$$

With C_0=C_1 and a parameter α=1/2 that corresponds to the thermalized accumulation of freely diffusing ions according to their electrochemical potential. However, the experimental observations reported in Fig. 5 show that α=1/2 is far from being satisfied. Since α ~0.02, as shown in Fig 5(b), it is apparent that the rise of capacitance does not correspond simply to the thermalized distribution of ions, but to an exponential distribution of states characterized by a temperature parameter T_0 as α=T/T_0.[42] This exponential distribution of states is a common occurrence in ionic and electronic systems that are characterized by a large degree of disorder. For example, a distribution of states has been observed in the intercalation of Li^+ ions into WO_3 electrochromic thin films[43] and also for the insertion of Li into ultrathin Ge layer in Si/Ge battery cathodes.[44]

The observation of an exponential density of states (DOS) for the accumulation of ions close to the perovskite/Au electrode interface indicates that ions become immobilized in the host material with the given distribution. According to the observation of the large changes of capacitance reported above, we can assume that

such a distribution is not intrisically formed at the interface but rather has been caused by the prolonged voltage applied to the symmetric cell. Therefore, a special layer is formed at the interface which is richer in I_2 and reduces the ability to take ions from the bulk. Tentatively we assume that reaction at the metal surface produces a film of PbI_2 that contains the exponential distribution suggested in Eq. (6). This observation would consistent with the formation of a PbI_2 layer under a continuous electrical bias.[33]

2.3. Photoluminescence Characterization within Iodine Vapor

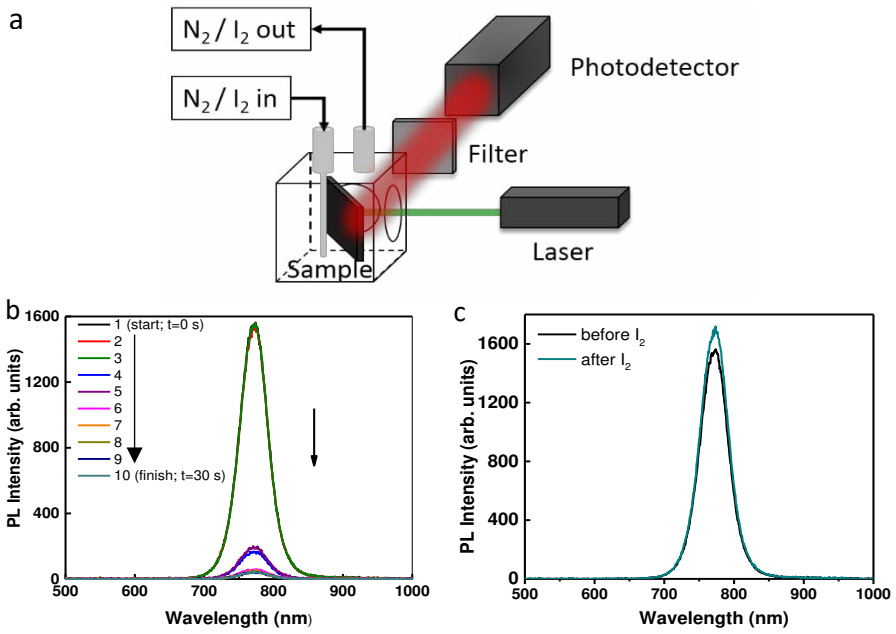

Figure 6. a) Schematic diagram of the PL quenching/recovery experiment using I_2 saturated N_2 and pure N_2 vapor, respectively. The excitation source is a laser with wavelength of 532 nm. b) Temporal evolution of the PL intensity of a perovskite film in I_2 vapor. PL spectra were recorded every 3 sec. c) Recovery of PL intensity of perovskite film after 5 min in a pure N_2 atmosphere.

To further understand the role of iodide ions on the PL performance of device, we carried out a time dependent PL under an iodine vapor atmosphere with configuration displayed in Fig 6(a). As shown in Fig 6(b), as the I_2 vapor (mixed with N_2 gas flow)

was introduced into the chamber, the PL intensity immediately decreases. After 30 sec, the PL intensity decreased by around 2 orders magnitude. Then the I_2 saturated gas was turned off and the chamber was purged with pure N_2 leading to a recovery of the PL intensity to its original value after ~5 min. The optical absorption of iodide vapor[45] does not affect the excitation (532 nm) or the emission signal (~780 nm) (Figure S9). This PL quenching is only associated with the influence of iodine doping in the perovskite film. The detailed microscopic process is still under investigation, however this rather simple experiment elucidates the direct and reversible influence of accumulated iodide.

2.4. Model of Photoluminescence Quenching under External Electrical Fields

Now, we can provide a picture on the evolution of PL dark areas on the perovskite film under external electrical field. This enhanced non-radiative recombination pathway includes both the trap-assisted recombination[46] and possible Auger-like recombination due to the charged mobile defects.[17, 20] Under external fields, the mobile ions obtain sufficient energy to overcome the activation energy[32, 47] and start to drift. These accumulated charges enhance the local electrical field.[14] It is known that the excited states are significantly influenced by its surrounding, *e.g.* ionized grains,[48] which results in the PL quenching.[20, 49] Here, it is necessary to mention that during this experiment, we cannot completely rule out the migration or reorientation of MA^+ ions under an electrical field,[16, 50] though the recent evidences in literatue point toward iodine.

The exact ionic migration pathway is still unclear. Due to the large density of defect states in the perovskite film, ascribed to the low-temperature film fabrication, the

defect facilitated ion migration may play an important role. Recently, more and more evidence indicates that the grain boundary, where large amount of defects exist due to the lack of perfect crystalline structure, serves as the main ionic migration channel.[22, 51] In addition, a different case is observed when the ion does not act merely as an spectator but lead to chemical reactions with the surrounding materials. Obviously, in this case the rate of the reactions may be limited by the ions supply and this will follow diffusive limitations. In the case of perovskite solar cells, it looks like we are able to remove 1-3 iodide ions from each unit cell according to previous results.[52]

It is necessary to mention that the moving front in Fig. 2 might not be actually ions migration but the reaction product between the perovskite and the excess ions. In fact, this impressive flat profile of the fronts as shown in Figure 2 are not usually observed in diffusive processes and rather implies that a certain threshold value of accumulated iodine is responsible for this phenomenon

3. Conclusion

In conclusion, we demonstrate a direct method to visualize ion migration in an electric field in organolead halide perovskite films through wide-field PL imaging microscopy. It is evident that local stoichiometric variations due to external electrical field have a significant impact on the local PL performance, and therefore influence the solar cells performance. This field driven inhomogeneity is associated with the iodide ions migration, which is confirmed by both the IS characterization and PL quenching under I_2 vapor. By employing PL imaging microscopy in combination with IS, we further characterize dynamic process of these iodide ions when monitoring the migration of PL inactive area under external electrical field in lateral-configured

electrode device. Hence, PL imaging microscopy provides an *in-situ* approach to investigate the ionic migration, which has obvious impact on photovoltaic performance, such as *J-V* hysteresis and chemical degradation. This provides a powerful tool to investigate the influence of grain boundaries, crystal size or passivation procedures in perovskite thin films. To further improve the performance and stability of perovskite solar cells, it is important to carefully control the defect/ions migration within the operating device, either by decreasing the defect density in the bulk (crystalline size and quality) or alleviating the long-term biasing effect in the vicinity of electrode.

4. Experimental Section

Perovskite solar cells Device Fabrication and Characterization. CH_3NH_3I (MAI) was purchased from Tokyo Chemical Industry (TCI) company, and Spiro-OMeTAD (2,2',7,7'-Tetrakis-(N,N-di-4-methoxyphenylamino)-9,9'-spirobifluorene) was purchased from Merck company. All the other chemicals were purchased from Sigma-Aldrich and were used as received.

Fluorine-doped tin oxide ($F:SnO_2$) transparent conducting glasses were cut and patterned by Zn power and HCl solution. FTO glasses were washed with acetone, 2% hellmanex diluted in deionized water, deionized water and isopropanol successively for 10 min each. Then by spraying a solution of Titanium diisopropoxide bis(acetylacetonate) (0.6 mL) in ethanol (21.4 mL) at 450 ℃ for 90 min in ambient atmosphere, a compact TiO_2 layer (~ 50 nm) was deposited.

MAI and lead chloride ($PbCl_2$) (3:1 molar ratio) was dissolved in anhydrous N,N-Dimethylformamide (DMF). Then, this precursor solution was spin-coated on the TiO_2/FTO substrates at 3000 rpm for 60 s. After drying for approximately 30 min, the as-spun films were annealed at 100 ℃ for 90 min. Following that, Spiro-OMeTAD solution was prepared by dissolving 72.3 mg Spiro-OMeTAD, 26.3 μL Lithium-bis(trifluoromethanesulfonyl)imide (Li-TFSI) solution (520 mg Li-TFSI in 1 mL acetonitrile), and 43.2 μL 4-tert-butylpyridine in 1 mL chlorobenzene. This hole transport layer (HTL) was deposited by spin-coating at 4000 rpm for 30 s. All device fabrication steps were carried out within a nitrogen gas filled glovebox. The whole of the device was exposed in a dry box (ambient atmosphere with humidity < 5%) for more than 12h. Finally, a 150 nm silver electrode was deposited by thermal evaporation in a chamber with a pressure of approximately 1×10^{-6} mbar. The effective electrode area was 9 mm^2 or 16 mm^2.

J-V measurements were performed under inert environment with a Keithley 2400 source measure unit under 100 mW/cm^2 illumination from an AM 1.5 solar simulator. The active area of 4 mm^2 and 9 mm^2 were defined by the overlap of a black mask aperture area, the FTO and the evaporated top electrode. The light intensity was calibrated before by a Silicon detector. There was no pre-biasing process. The scanning speed is 0.9 V/s.

Perovskite Film Fabrication for PL imaging Experiment. The similar procedure was used to fabricate the film for the PL imaging characterization. Glass substrates were washed with acetone, and isopropanol successively for 10 min each. Then these glass substrates were treated with Ozone for around 10 min. Following that, in a nitrogen

glovebox, perovskite precursor was spin-coated on glass substrates at 3000 rpm for 60 s. These as-spun films were subsequently annealed at 100 ℃ for 60 min in glovebox. In the end, a 40 mg/mL poly(methyl methacrylate) (PMMA) solution dissolved in butyl acetate (anhydrous, 99%) was then spin-coated on the perovskite film as a protection layer, at speed of 2000 rpm for 60 sec.

For the experiment of PL imaging under electrical field, perovskite film on glasses were transferred into an evaporation chamber with pressure of 1×10^{-6} mbar, and ~100 nm thickness of gold was deposited by thermal evaporation through a shadow mask. The electrode distance was 200 μm and the interdigitating electrode geometry provided a ratio between channel width W and length L, W/L of 500.

PL imaging experiment. The setup used for PL imaging of perovskite films was based on a home-built confocal microscope. The specimen was illuminated by a green laser (wavelength with 532 nm), resulting in excitation of free charge carriers. With emission filter, the emission signal can be separated from the excitation light using emission suitable filters, and is finally collected by a detector.

In this project, the excitation source was a pulsed diode laser (LDH-P-C-4508B, Picoquant: 20 MHz repetition rate, 70 ps pulse duration). The excitation power can be modulated by Neutral Density attenuation filters. The excitation power illuminated on the film was ~40 mW/cm^2. The laser light was spatially filtered and directed to the microscope which was equipped with an infinity-corrected high-numerical-aperture oil-immersion objective (60×, numerical aperture of 1.45, Olympus). The perovskite

film was placed in the focal plane of the objective lens, and the sample position was controlled by a piezo-stage (Tritor 102 SG, from piezosystem Jena).

For imaging, the PL signal was collected by the same objective, passed a long-pass filter (LP545, AHF) to suppress residual laser light, and was imaged onto a charge-coupled device (CCD) camera (Orca-ER, Hamamatsu). An additional lens (widefield lens) was flipped into the excitation beam path to focus the laser light into the back focal plane of the microscope objective. This allowed for illumination of a large area with ~ 60 µm diameter in the sample plane. For electric field dependent measurement (viedo), the PL was recorded with a constant 20 V dc voltage being applied between the Au electrodes.

Impedance spectroscopy. The setup to measure impedance spectroscopy is similar to that described previously for PL analysis. However, in this case the dc voltage source to polarize the sample was a potentiostat equipped with a frequency analyser (Zahner Potentiostat, Zenium). A small ac perturbation was applied and the differential current output was measured to calculate the impedance response. The frequency window was kept small ranging between 10 kHz-100mHz to minimize the measurement time. Each frequency scan took less than 1 minute and a delay time of 5 minutes was used between scans to carry out the PL measurements. The light source was turned off after the PL measurement and the new IS scan was taken under dark conditions. For measurements at a dc voltage of 2 V the delay time was reduced to 30 seconds and this enabled the observation of the accumulation of ions at the interface. Alternatively, devices where measured systematically under a range of applied bias using a high

sensitivity potentiostat (Autolab PGSTAT-30) to cover a lower frequency ranged down to 5 mHz.

PL under iodine atmosphere. We measured the PL of a perovskite film under iodine atmosphere. For this, a perovskite film was placed in an atmospherically sealed measuring chamber with quartz glass windows. Before starting the measurement, we heated the chamber to roughly 50 °C using a heatgun in order to prevent condensation of solid iodine onto the windows and the perovskite film. The photoluminescence measurements under iodine were performed using an 80 mW laser (PGL V – II) with a wavelength of 532 nm. The spectra were recorded using a spectrometer (QE Pro from Ocean Optics) and matching optical fibre. A filter (OG 590 nm) was used to filter the emission light.

Initially the PL was measured under a pure nitrogen atmosphere to obtain a reference value. Subsequently a vial with solid iodine was connected to the gas inlet pipeline and thus the chamber was filled with a mixed iodine/nitrogen atmosphere. Upon connecting the iodine vapor, we measured a PL spectrum every three seconds to observe the progress of the PL intensity. After the PL intensity stabilized on a lower level, we disconnected the iodine from the gas pipeline and flushed the measurement chamber with pure nitrogen.

Acknowledgement

Financial support by the Bavarian State Ministry of Science, Research, and the Arts for the Collaborative Research Network ‘‘Solar Technologies go Hybrid’’ and Federal Ministry of Education and Research BMBF (03SF0484C) are gratefully

acknowledged. RH, JK, and CAML acknowledge additional funding from the German Research Foundation DFG (GRK1640 and HI1508/2). Part of this research has been carried out at the Australian Synchrotron at the SAXS/WAXS beamline. A.G. and J.B. acknowledge funding from MINECO of Spain (MAT2016-76892-C3-1-R and RYC-2014-16809) and Generalitat Valenciana Project PROMETEOII/2014/020. We are thankful to Konstantin Deichsel and Jürgen Köhler for their experimental support with the PL measurements.

References:

[1] A. Kojima, K. Teshima, Y. Shirai, T. Miyasaka, *J. Am. Chem. Soc.* **2009**, *131*, 6050.
[2] W. S. Yang, J. H. Noh, N. J. Jeon, Y. C. Kim, S. Ryu, J. Seo, S. I. Seok, *Science* **2015**, *348*, 1234.
[3] T. C. Sum, N. Mathews, *Energy Environ. Sci.* **2014**, *7*, 2518; Y.-C. Hsiao, T. Wu, M. Li, Q. Liu, W. Qin, B. Hu, *J. Mater. Chem. A* **2015**, *3*, 15372.
[4] S. D. Stranks, H. J. Snaith, *Nat. Nanotechnol.* **2015**, *10*, 391.
[5] K. Tvingstedt, O. Malinkiewicz, A. Baumann, C. Deibel, H. J. Snaith, V. Dyakonov, H. J. Bolink, *Sci. Rep.* **2014**, *4*, 6071; A. Filippetti, P. Delugas, A. Mattoni, *J. Phys. Chem. C* **2014**, *118*, 24843; W. E. I. Sha, X. Ren, L. Chen, W. C. H. Choy, *Appl. Phys. Lett.* **2015**, *106*, 221104; W. Tress, N. Marinova, O. Inganäs, M. K. Nazeeruddin, S. M. Zakeeruddin, M. Graetzel, *Adv. Energy Mater.* **2015**, *5*, 1400812.
[6] Y. Yamada, T. Nakamura, M. Endo, A. Wakamiya, Y. Kanemitsu, *J. Am. Chem. Soc.* **2014**, *136*, 11610.
[7] L. M. Herz, *Annu. Rev. Phys. Chem.* **2015**, *67*, 65.
[8] N. K. Noel, A. Abate, S. D. Stranks, E. S. Parrott, V. M. Burlakov, A. Goriely, H. J. Snaith, *ACS Nano* **2014**, *8*, 9815.
[9] W. Shockley, H. J. Queisser, *J. Appl. Phys.* **1961**, *32*, 510.
[10] O. D. Miller, E. Yablonovitch, S. R. Kurtz, *IEEE J. Photovolt.* **2012**, *2*, 303.
[11] Z.-K. Tan, R. S. Moghaddam, M. L. Lai, P. Docampo, R. Higler, F. Deschler, M. Price, A. Sadhanala, L. M. Pazos, D. Credgington, F. Hanusch, T. Bein, H. J. Snaith, R. H. Friend, *Nat. Nanotechnol.* **2014**, *9*, 687; J. Wang, N. Wang, Y. Jin, J. Si, Z.-K. Tan, H. Du, L. Cheng, X. Dai, S. Bai, H. He, Z. Ye, M. L. Lai, R. H. Friend, W. Huang, *Adv. Mater.* **2015**, *27*, 2311.
[12] F. Deschler, M. Price, S. Pathak, L. E. Klintberg, D.-D. Jarausch, R. Higler, S. Hüttner, T. Leijtens, S. D. Stranks, H. J. Snaith, M. Atatüre, R. T. Phillips, R. H. Friend, *J. Phys. Chem. Lett.* **2014**, *5*, 1421.

[13] W. d. Dane, S. M. Vorpahl, S. D. Stranks, H. Nagaoka, G. E. Eperon, M. E. Ziffer, H. J. Snaith, D. S. Ginger, *Science* **2015**, *348*, 683.
[14] S. Chen, X. Wen, R. Sheng, S. Huang, X. Deng, M. A. Green, A. Ho-Baillie, *ACS Appl. Mater. Inerfaces* **2016**, *8*, 5351.
[15] J. F. Galisteo-López, M. Anaya, M. E. Calvo, H. Míguez, *J. Phys. Chem. Lett.* **2015**, *6*, 2200.
[16] R. Gottesman, L. Gouda, B. S. Kalanoor, E. Haltzi, S. Tirosh, E. Rosh-Hodesh, Y. Tischler, A. Zaban, C. Quarti, E. Mosconi, F. De Angelis, *J Phys. Chem. Lett.* **2015**, *6*, 2332.
[17] X. Deng, X. Wen, C. F. J. Lau, T. Young, J. Yun, M. A. Green, S. Huang, A. W. Y. Ho-Baillie, *J. Mater. Chem. C* **2016**, *4*, 9060.
[18] D. L. Jacobs, M. A. Scarpulla, C. Wang, B. R. Bunes, L. Zang, *J. Phys. Chem. C* **2016**, *120*, 7893.
[19] Y. Lin, L. Shen, J. Dai, Y. Deng, Y. Wu, Y. Bai, X. Zheng, J. Wang, Y. Fang, H. Wei, W. Ma, X. C. Zeng, X. Zhan, J. Huang, *Adv. Mater.* **2017**, *29*, DOI: 10.1002/adma.201604545.
[20] X. Wen, A. Ho-Baillie, S. Huang, R. Sheng, S. Chen, H.-c. Ko, M. A. Green, *Nano Lett.* **2015**, *15*, 4644.
[21] S. D. Stranks, G. E. Eperon, G. Grancini, C. Menelaou, M. J. P. Alcocer, T. Leijtens, L. M. Herz, A. Petrozza, H. J. Snaith, *Science* **2013**, *342*, 341.
[22] Y. Yuan, J. Huang, *Acc. Chem. Res.* **2016**, *49*, 286.
[23] S. Ravishankar, O. Almora, C. Echeverría-Arrondo, E. Ghahremanirad, C. Aranda, A. Guerrero, F. Fabregat-Santiago, A. Zaban, G. Garcia-Belmonte, J. Bisquert, *J. Phys. Chem. Lett.* **2017**, *8*, 915.
[24] Z. Hameiri, A. Mahboubi Soufiani, M. K. Juhl, L. Jiang, F. Huang, Y.-B. Cheng, H. Kampwerth, J. W. Weber, M. A. Green, T. Trupke, *Prog. Photovolt: Res. Appl.* **2015**, *23*, 1697; A. M. Soufiani, Z. Hameiri, S. Meyer, S. Lim, M. J. Y. Tayebjee, J. S. Yun, A. Ho-Baillie, G. J. Conibeer, L. Spiccia, M. A. Green, *Adv. Energy Mater.* **2016**, DOI: 10.1002/aenm.201602111.
[25] J. M. Azpiroz, E. Mosconi, J. Bisquert, F. De Angelis, *Energy Environ. Sci.* **2015**, *8*, 2118.
[26] B. Chen, M. Yang, X. Zheng, C. Wu, W. Li, Y. Yan, J. Bisquert, G. Garcia-Belmonte, K. Zhu, S. Priya, *J Phys. Chem. Lett.* **2015**, *6*, 4693.
[27] A. T. Haedler, K. Kreger, A. Issac, B. Wittmann, M. Kivala, N. Hammer, J. Kohler, H.-W. Schmidt, R. Hildner, *Nature* **2015**, *523*, 196; A. Issac, R. Hildner, C. Hippius, F. Würthner, J. Köhler, *ACS Nano* **2014**, *8*, 1708; C. Li, Y. Zhong, C. Luna, T. Unger, K. Deichsel, A. Gräser, J. Köhler, A. Köhler, R. Hildner, S. Huettner, *Molecules* **2016**, *21*, 1081.
[28] Y. Tian, M. Peter, E. Unger, M. Abdellah, K. Zheng, T. Pullerits, A. Yartsev, V. Sundstrom, I. G. Scheblykin, *Phys. Chem. Chem. Phys.* **2015**, *17*, 24978; H.-H. Fang, F. Wang, S. Adjokatse, N. Zhao, M. A. Loi, *Adv. Funct. Mater.* **2016**, *26*, 4653.
[29] R. Gottesman, A. Zaban, *Acc. Chem. Res* **2016**, *49*, 320.
[30] C. Li, S. Tscheuschner, F. Paulus, P. E. Hopkinson, J. Kießling, A. Köhler, Y. Vaynzof, S. Huettner, *Adv. Mater.* **2016**, *28*, 2446.
[31] C. Eames, J. M. Frost, P. R. F. Barnes, B. C. O'Regan, A. Walsh, M. S. Islam, *Nat. Commun.* **2015**, *6*, 7497.
[32] S. Meloni, T. Moehl, W. Tress, M. Franckevicius, M. Saliba, Y. H. Lee, P. Gao, M. K. Nazeeruddin, S. M. Zakeeruddin, U. Rothlisberger, M. Graetzel, *Nat. Commun.* **2016**, *7*, 10334.

[33] Y. Yuan, Q. Wang, Y. Shao, H. Lu, T. Li, A. Gruverman, J. Huang, *Adv. Energy Mater.* **2016**, *6*, 1501803.
[34] Z. Xiao, Y. Yuan, Y. Shao, Q. Wang, Q. Dong, C. Bi, P. Sharma, A. Gruverman, J. Huang, *Nat. Mater.* **2015**, *14*, 193.
[35] S. M. Sze, *Physics of Semiconductor Devices* **1981**, Wiley.
[36] Y. Yuan, J. Chae, Y. Shao, Q. Wang, Z. Xiao, A. Centrone, J. Huang, *Adv. Energy Mater.* **2015**, *5*, 1500615.
[37] T.-Y. Yang, G. Gregori, N. Pellet, M. Grätzel, J. Maier, *Angew. Chem. Int. Ed.* **2015**, *54*, 7905.
[38] J. Carrillo, A. Guerrero, S. Rahimnejad, O. Almora, I. Zarazua, E. Mas-Marza, J. Bisquert, G. Garcia-Belmonte, *Adv. Energy Mater.* **2016**, *6*, 1502246.
[39] O. Almora, A. Guerrero, G. Garcia-Belmonte, *Appl. Phys. Lett.* **2016**, *108*, 043903.
[40] R. S. Sanchez, V. Gonzalez-Pedro, J.-W. Lee, N.-G. Park, Y. S. Kang, I. Mora-Sero, J. Bisquert, *J. Phys. Chem. Lett.* **2014**, *5*, 2357.
[41] K. B. Oldham, *J. Electroanal. Chem.* **2008**, *613*, 131.
[42] J. Bisquert, *Nanostructured energy devices: Equilibrium concepts and kinetics* **2014**, CRC Press.
[43] M. Strømme Mattsson, *Phys. Rev. B* **1998**, *58*, 11015.
[44] M. Haro, T. Song, A. Guerrero, L. Bertoluzzi, J. Bisquert, U. Paik, G. Garcia-Belmonte, *Phys. Chem. Chem. Phys.* **2014**, *16*, 17930.
[45] S. George, N. Krishnamurthy, *Am. J. Phys.* **1989**, *57*, 850.
[46] G.-J. A. H. Wetzelaer, M. Scheepers, A. M. Sempere, C. Momblona, J. Ávila, H. J. Bolink, *Adv. Mater.* **2015**, *27*, 1837.
[47] H. Yu, H. Lu, F. Xie, S. Zhou, N. Zhao, *Adv. Funct. Mater.* **2016**, *26*, 1411.
[48] P. Anger, P. Bharadwaj, L. Novotny, *Phys. Rev. Lett.* **2006**, *96*, 113002.
[49] A. L. Efros, M. Rosen, *Phys. Rev. Lett.* **1997**, *78*, 1110.
[50] C. Qiu, J. K. Grey, *J Phys. Chem. Lett.* **2015**, *6*, 4560.
[51] Y. Shao, Y. Fang, T. Li, Q. Wang, Q. Dong, Y. Deng, Y. Yuan, H. Wei, M. Wang, A. Gruverman, J. Shield, J. Huang, *Energy Environ. Sci.* **2016**, *9*, 1752; J. S. Yun, J. Seidel, J. Kim, A. M. Soufiani, S. Huang, J. Lau, N. J. Jeon, S. I. Seok, M. A. Green, A. Ho-Baillie, *Adv. Energy Mater.* **2016**, *6*, 1600330.
[52] E. Mosconi, D. Meggiolaro, H. J. Snaith, S. D. Stranks, F. De Angelis, *Energy Environ. Sci.* **2016**, *9*, 3180.